Entire mission striping assessment for SNPP, NOAA-20 and NOAA-21 VIIRS

Tiejun Chang[a*] and Xiaoxiong Xiong[b]

[a] Science Systems and Applications, Inc, Lanham, MD 20706
[b] Sciences and Exploration Directorate, NASA/GSFC, Greenbelt, MD 20771

Abstract

The Visible Infrared Imaging Radiometer Suite (VIIRS) instruments aboard the Suomi NPP (SNPP), NOAA-20 (N20), and NOAA-21 (N21) spacecraft have successfully provided Earth image products since 2011, 2017, and 2022, respectively. VIIRS has 22 bands with resolutions of 375 m and 750 m for the imaging and moderate resolution bands, respectively, covering a spectral range of 400-12,490 nm. Among them, moderate bands (M-band) 1 to 11 and imaging bands (I-band) 1 to 3 are reflective solar bands (RSBs), and M12 to M16 and I4 and I5 are thermal emissive bands (TEB). Each M-band has 16 detectors, and each I-band has 32 detectors. M-bands (1-5, 7, and 13) have dual-gain stages to enhance the measurement dynamic range. The nonlinear responses of RSB and TEB detectors were characterized during pre-launch testing. An on-board solar diffuser tracks any linear response degradation for RSB detectors. For TEB detectors, an on-board blackbody (BB) tracks linear response change, and a scheduled BB warmup and cooldown event is used to monitor the non-linearity change. Unknown biases or uncertainty in the linear or nonlinear calibration coefficients between different detectors can cause unwanted striping in the image product. In this work, the striping is assessed for all RSB and TEB of the three VIIRS instruments on SNPP, N20, and N21. The assessment is performed using the NASA Level 1B reflectance and radiance products over the entire globe to analyze the aggregate striping and any changes over time. For each band of the three instruments, the striping assessment is performed at different signal levels to analyze their nonlinearity. The striping assessment is also performed separately for both gain stages of the dual-gain bands. The motivation of this work is to have a comprehensive understanding of VIIRS striping and its signal dependency to support calibration improvements and to reduce the striping over a broad radiance range.

Keywords: VIIRS, radiometric calibration, Striping

INTRODUCTION

The Visible Infrared Imaging Radiometer Suite (VIIRS) is a key instrument for the S-NPP and JPSS missions. The S-NPP was launched in October 2011, JPSS-1 (NOAA-20/N-20) in November 2017, and the JPSS-2 (NOAA-21/N21) in November 2022 [1-9]. The VIIRS has 22 spectral bands, including a day and night band (DNB), 14 reflective solar bands (RSB), M1-M11 and I1-I3 covering wavelengths from 0.41 to 2.2 μm, and 7 thermal emissive bands (TEB), M12-M16 and I4-I5 covering wavelengths from 3.7 to 12 μm. Among them, M1-M5, M7, and M13 are the dual gain bands. The on-board calibrators (OBC) solar diffuser (SD) and solar diffuser stability monitor (SDSM) are used for RSB and DNB calibrations, and the blackbody (BB) is for TEB calibration. The space view (SV) port is an extension of the nadir opening for background signal measurement and lunar observation [1]. Most RSB detectors (except for the SWIR bands) are located on VIS/NIR focal plane which is a warm focal plane operating at about instrument temperature, while the SWIR and TEB detector arrays are located on S/MWIR and LWIR cold focal plane assemblies (CFPAs) which are maintained at about 80 K for nominal operation by a passive cryo-radiator cooler. The VIIRS RSB calibration is routinely conducted by the SD and a solar diffuser stability monitor (SDSM). The scheduled lunar observations are also used for

RSB detector gain calibration. The VIIRS TEB calibration is performed using BB on scan-by-scan basis. For both RSB and TEB, the detector nonlinearities are calibrated in the pre-launch test. A special BB warm-up/cool-down (WUCD) event is performed regularly to characterize on-orbit detector nonlinearity for the TEB.

In general, the striping is caused due to inadequacy in the calibration algorithm. The assessment of the striping in L1B product can be beneficial for calibration algorithm improvement. The striping dependency on signal level and gain stage will also be very helpful for nonlinear calibration algorithm improvement. In this paper, the striping in both RSB and TEB have been assessed using Fourier Transform (FT) concept. Section 2 presents the assessment method and data processing. Sections 3 and 4 present VIIRS RSB and TEB striping performance for SNPP, N20, and N21.

2. STRIPING ASSESSMENT

2.1 Methodology

Traditionally, large-samples sized uniform scenes have been used for striping assessment, such as deserts used for RSB striping assessment. A statistical analysis of the measurements over certain scenes can also be used for detector differences, such as over deep convective clouds (DCC) and desert [10-12]. The average of sufficient measurement data over well characterized scene as DCC can be used for the detector difference at that signal level. A histogram method for the statistical analysis of large amount measurement data can also be used for striping assessment. This method provides an overall assessment of the detector differences over a large area. The counts over each measurement range of each detector can indicate the detector difference. These three methods have been applied to MODIS and VIIRS RSB striping assessments. For VIIRS TEB, the detector spectral response function difference can also be used to assess its impact on the detector difference [13]. In this paper a Fourier Transform based method is used to assess the detector difference for VIIRS RSB and TEB.

2.2 Data processing

The Fast-Fourier Transform (FFT) is the widely used image processing technique that can be used for striping assessment. The advantage of this method is to analyze any area of image as long as the data amount is sufficient. It can be used to assess striping dependency on signal level and other conditions. The striping assessment is performed for VIIRS RSB and TEB on SNPP, N20, and N21. The NASA LSIPS VIIRS L1B data is used in this work. To avoid the bowtie effect, only the center zone (zone 3) pixels are used. As this statistical analysis requires a large amount of measurement data, two-orbits of data from each month over the entire mission of the three instruments are used. Only the M-bands have been processed, but the same method can also be applied to the I bands. For RSB, the daytime measurements are processed, while for TEB, both the daytime and the nighttime data are processed.

There are two methods to compose an array for Fourier Transform for the detector difference analysis. One is to an average an array for zone 3 pixels in the along scan direction. The second is to append all the zone 3 along track pixels to one long array. The purpose of using these two processes is to construct an array for detector difference analysis using Fourier Transform. The results of these two methods are not identical. The resolution of Fourier Transform depends on the length of the array. A longer array gives a finer resolution. Since we know the spatial frequency, the two methods do not make too much difference. However, the appended long array takes more computation time for calculating the FFT. Theoretically, more the data processed, more accurate is the result for the detector difference since it is a statistical assessment. Considering the computation time, data amount, and measurement signal range coverage, in this work, the results come from two orbit measurement data. The two-orbits can cover different scene types such as ocean, land, snow, and ice. It also covers the reflectance with different solar angles which also affects the signal level.

The relative detector difference in radiance and reflectance is analyzed for RSB, while the relative radiance difference and absolute BT difference are analyzed for TEB. In this paper, the relative radiance difference is presented for RSB, and the BT difference is presented for TEB. The signal level dependency and gain stage

dependency are processed. For each dependency, the measurement data are separated into different groups depending on the signal level range or the detector gain stage. The processing is done for each group for the striping assessment to have the dependency.

For both RSB and TEB, the radiance measurement is used for signal level dependency, and the radiance range is determined from the range of measurement data. The entire range is divided into 10 group and the striping analysis is performed for each group. The reflectance dependency is also processed for RSB, and no significant difference is found compared to the radiance assessment. The brightness temperature (BT) is processed for TEB. The BT measurement data is divided into 10 groups from 200K to 300K with bin-size of 10K. Any group with pixel number for a detector exceeding 10000 is processed for striping assessment. Due to the BT range difference for different spectral bands, the group numbers processed are not identical. For each VIIRS instrument, two orbits Earth L1B data are selected for each month of entire mission. The results from two orbit data are used for striping assessment for that time, while all the results are used for the trending. In sections 3 and 4, the results of RSB radiance dependency and TEB BT dependency are presented in this paper.

3. VIIRS RSB STRIPING

3.1 SNPP VIIRS RSB

Figure 1 shows SNPP VIIRS RSB detector difference trending through the end of 2023. Each point is the relative radiance difference for each detector in a two orbit L1B daytime Earth measurement data. The relative radiance difference is insignificant for VIS bands in the early mission. The difference gradually increases, especially for band M2, and after 2019, the detector difference become larger for VIS bands. The SWIR bands show fluctuation of the detector difference. Overall, the striping effect is small for SNPP VIIRS RSB [12]. The SNPP VIIRS band M2 striping is processed for different radiance levels. Figure 2 shows the relative detector difference trending for SNPP VIIRS band M2 through the end of 2023. The detector relative difference is larger for high radiance level, especially for detector 1.

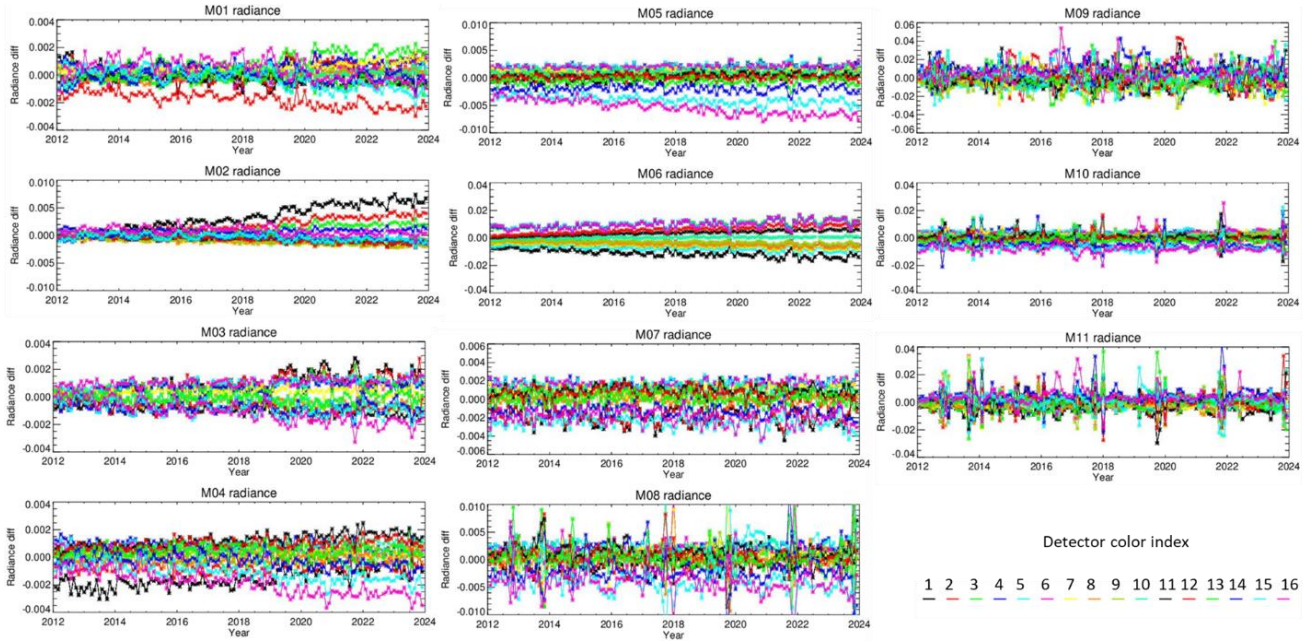

Figure 1. SNPP VIIRS RSB detector difference trending through the end of 2023. Each point is the relative radiance difference for each detector in a two orbit L1B daytime Earth measurement data.

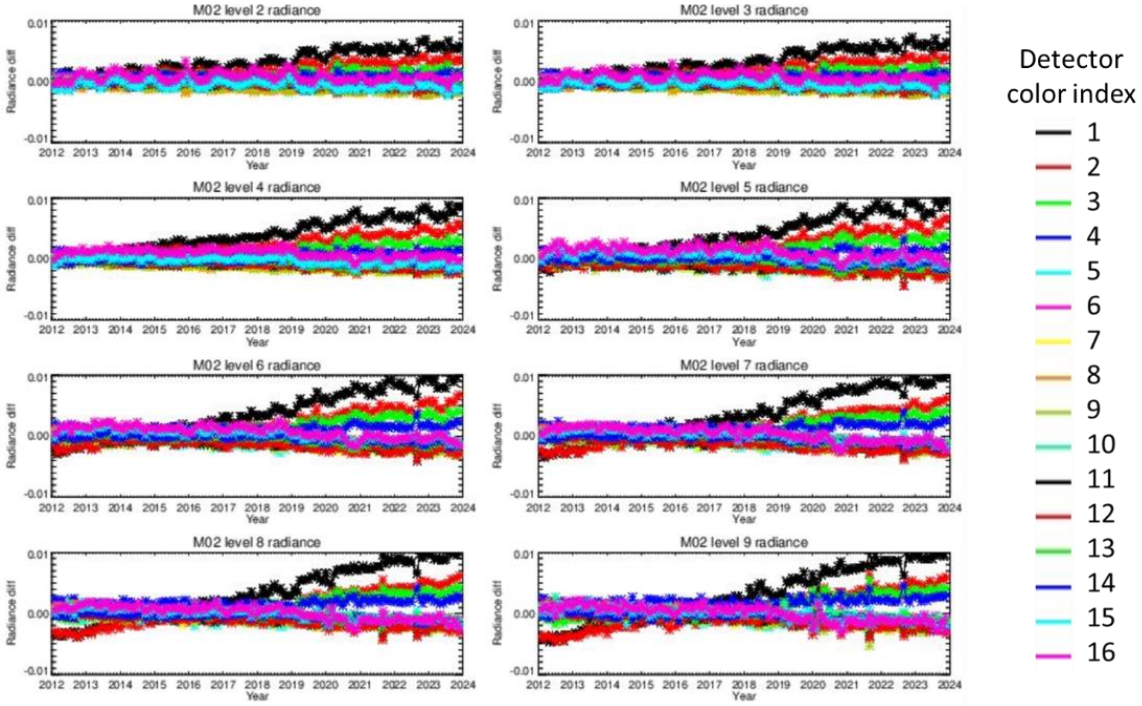

Figure 2. SNPP VIIRS band M2 striping radiance level dependency trending through the end of 2023. Each point is the relative radiance difference for each detector in a two orbit L1B Earth measurement data.

3.2 N20 VIIRS RSB

Figure 3 shows N20 VIIRS RSB detector difference trending through February 2024. Each point is the relative radiance difference for each detector in a two orbit L1B daytime Earth measurement data. The relative radiance difference is small for VIS bands in the early mission. The relative detector difference shows seasonal fluctuation for bands M1 and M2. It is also noticed that the detector difference is larger for 2023. The cause may be the difference in the polarization effect for short wavelength bands. On November 7, 2023, a destriping algorithm was applied for the N20 VIS/NIR bands in forward production of the L1B to address static striping seen in all VIS/NIR bands and a gradually increasing time-dependent striping in band M1. After this algorithm change, the detector difference is reduced significantly. The SWIR bands show fluctuation of the detector difference.

To show the detector difference seasonal oscillation, Figure 4 shows the detector difference radiance dependency for day 1 of 2023 and day 181 of 2023 for M1. M2, and M3. The major difference between these two results is the detector difference at low radiance level. At low radiance levels, the data is likely all from ocean scenes, where in the blue wavelength range a large portion of the top of atmosphere signal comes from atmospheric scattering. Striping can be introduced both from polarization sensitivity, which is different for each detector for N20 based on pre-launch measurements, and from real differences in atmospheric path length seen by the different detector locations on the focal plane [14]. For high radiance levels, the data is more likely coming from land and cloud scenes and the atmosphere effects contribute a smaller fraction of the total signal. Thus, the detector difference seasonal oscillation is much smaller for the higher radiance cases.

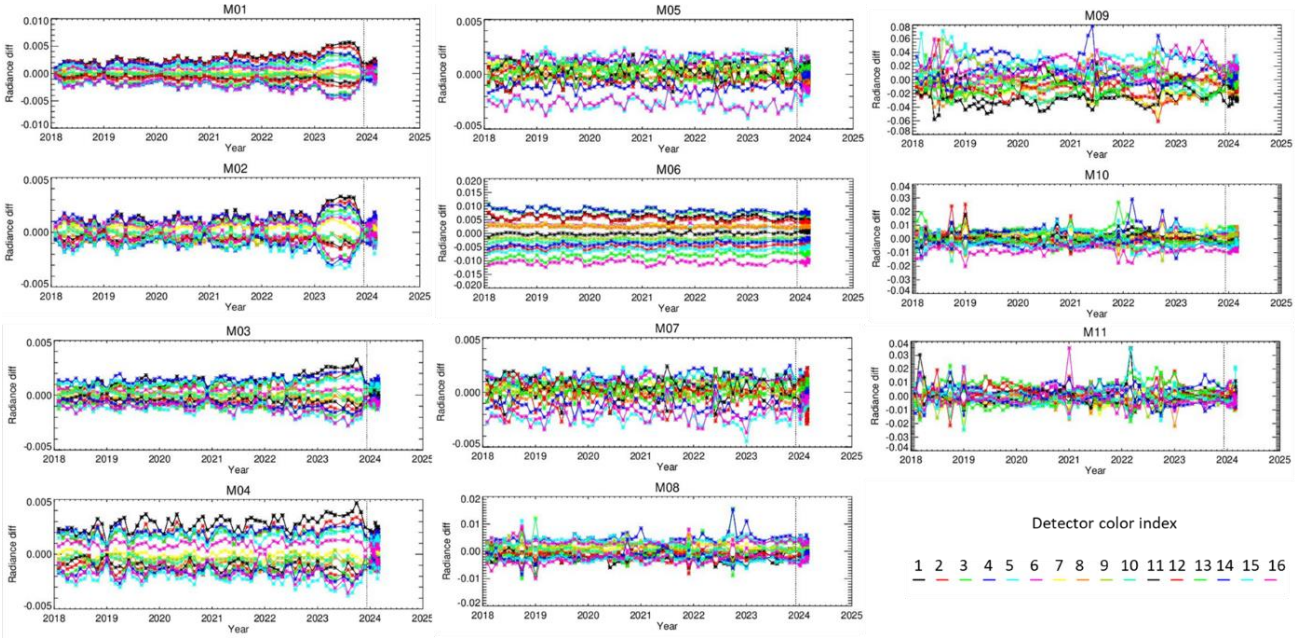

Figure 3. N20 VIIRS RSB detector difference trending till February 2024. Each point is the relative radiance difference for each detector in a two orbit L1B daytime Earth measurement data.

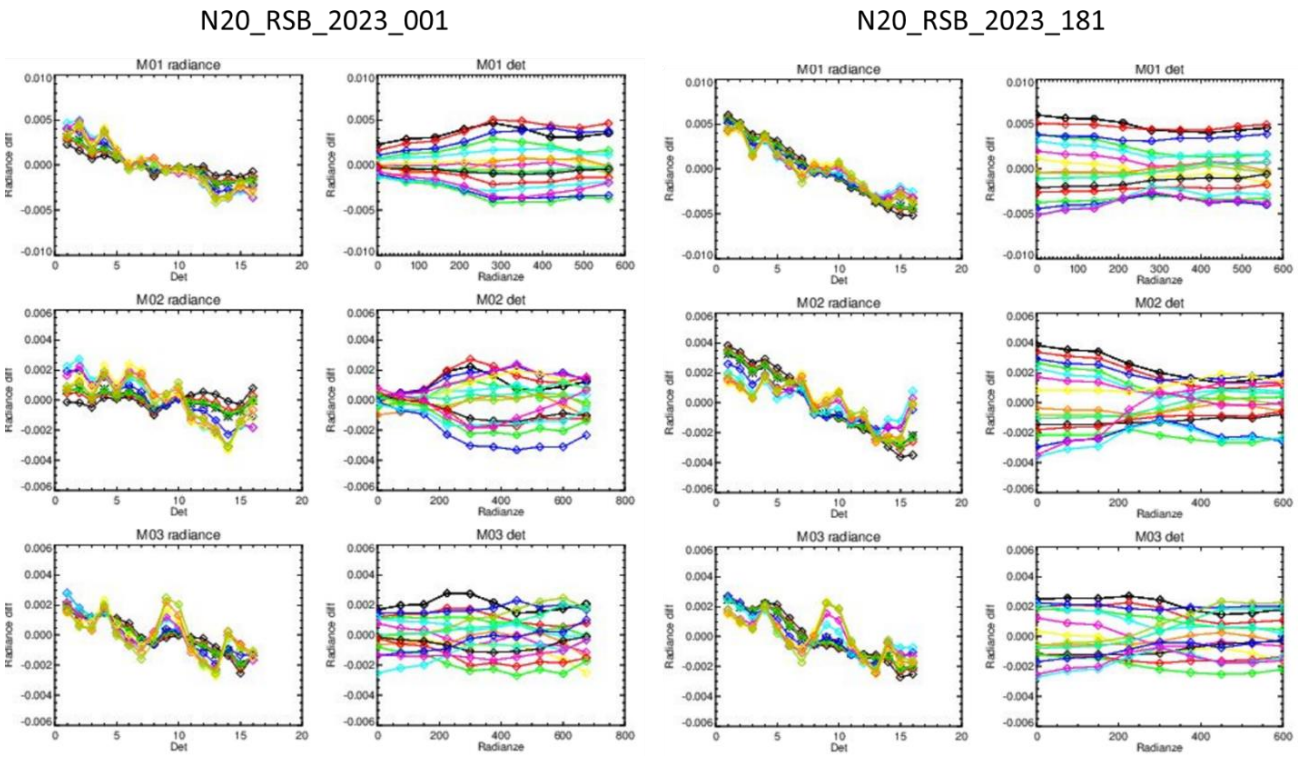

Figure 4. (Left panel) The detector difference dependency on radiance level for N20 VIIRS bands M1, M2, and M3 for day 1 in 2023. (right panel) The detector difference dependency on radiance level for N20 VIIRS bands M1, M2, and M3 for day 181 in 2023.

3.2 N21 VIIRS RSB

Figure 5 shows N21 VIIRS RSB detector difference trending through the end of 2023. Each point is the relative radiance difference for each detector in a two orbit L1B daytime Earth measurement data. The relative radiance difference is insignificant for VIS bands in the early mission. The difference gradually increased for bands M1, M2, M3, and M4. The SWIR bands show fluctuation of the detector difference. Overall, the striping effect is small for N21 VIIRS RSB. Figure 6 shows the detector difference radiance dependency for day 91 of 2023 and day 1 of 2024 to analyze the change for M1. M2, and M3. Generally, the change is not signal level dependent. The detector difference increases in time for all radiance levels. The striping assessment for N21 is performed on the Collection 2.0 version of NASA L1B data for N21. Recently, a calibration update has been made for an upcoming new Collection 2.1 (C2.1) L1B, including a VIS/NIR de-striping algorithm that is very similar to the de-striping algorithm previously used for SNPP [12] and N20, as well as several other improvements. The calibration look-up-tables for C2.1 were initially delivered in June 2024 and the L1B is expected to be released soon. The striping assessment will be performed for the C2.1 data after it is released to confirm the striping improvements.

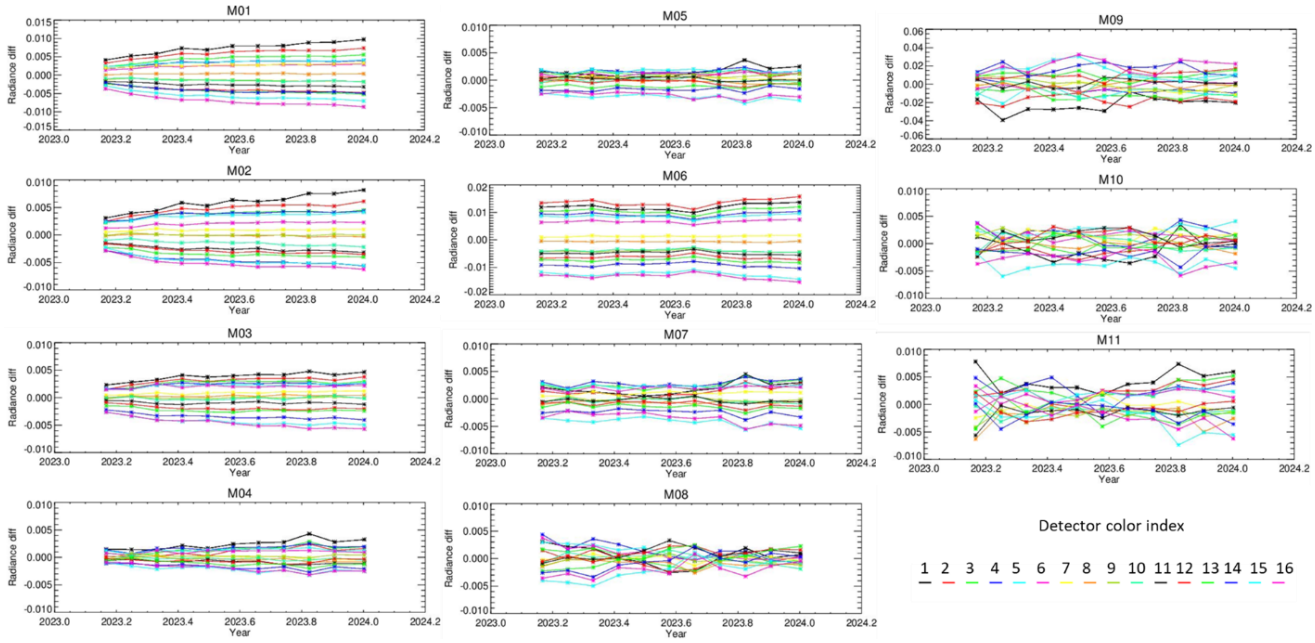

Figure 5. N21 VIIRS RSB detector difference trending till end of 2023. Each point is the relative radiance difference for each detector in a two orbit L1B daytime Earth measurement data.

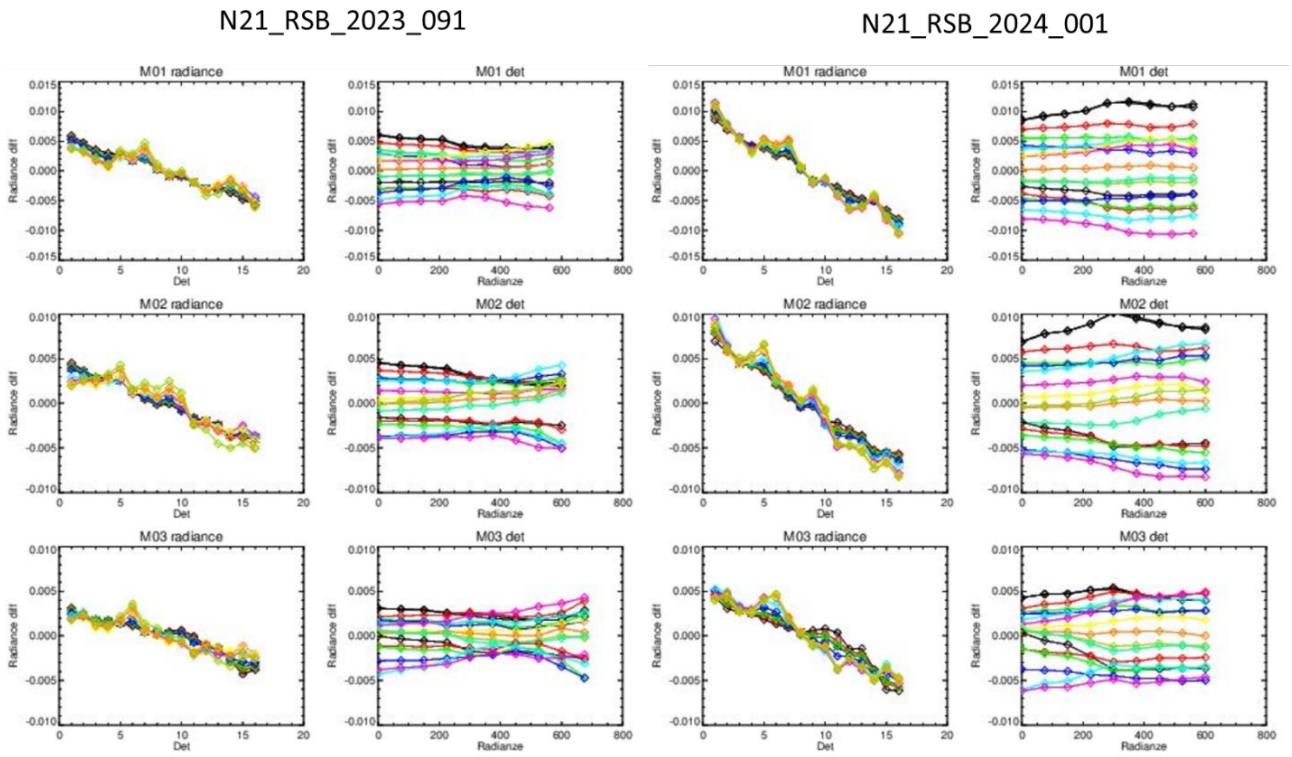

Figure 6. (Left panel) The detector difference dependency on radiance level for N21 VIIRS bands M1, M2, and M3 for day 91 of 2023. (right panel) The detector difference dependency on radiance level for N20 VIIRS bands M1, M2, and M3 for day 1 of 2024.

4. VIIRS TEB STRIPING

4.1 SNPP VIIRS TEB

The same method has been applied to TEB striping assessment for VIIRS on SNPP, N20, and N21. For TEB the signal level and detector difference are processed for BT and radiance. In this paper, the results are presented for the BT for both signal level and detector difference. It shows that the detector difference is stable over the mission, and the averaged detector difference over the mission can be used for striping assessment. Figure 7 shows SNPP VIIRS TEB detector difference trending through the end of 2023. Each point is the relative radiance difference for each detector in a two orbit L1B Earth measurement data. Figure 8 shows SNPP VIIRS TEB detector difference averaged over entire mission through the end of 2023. The left panel shows the average detector difference as function of scene BT. The vertical lines for M12 and M13 are the minimum temperature measurements in VIIRS specification. For M14 to M16, the minimum temperature in specification is 190K. The right panel shows the average detector difference for each detector. The vertical lines for M12 and M13 are the minimum temperature measurements in VIIRS specification. The detector difference is generally small for SNPP VIIRS TEB. Only the bands M12 and M13 show the noticeable detector difference for low BT scenes while the other bands detector difference is insignificant. As indicated in Figure 8, the minimum temperature specification is 230K. the detector difference is small above 230K. The edge pixels in zones 1 and 5 have larger noise, and the minimum temperature specification is for these pixels. The pixels in zone 3 are aggregated from 3 original pixels and the noise is lower than the edge pixels. The measurement can be lower than the minimum temperature specification. This analysis lower to 200K is helpful to understand the cause of the detector

difference and to make calibration improvement if needed. For the bands M14, M15, and M16, the minimum temperature specifications are 190K.

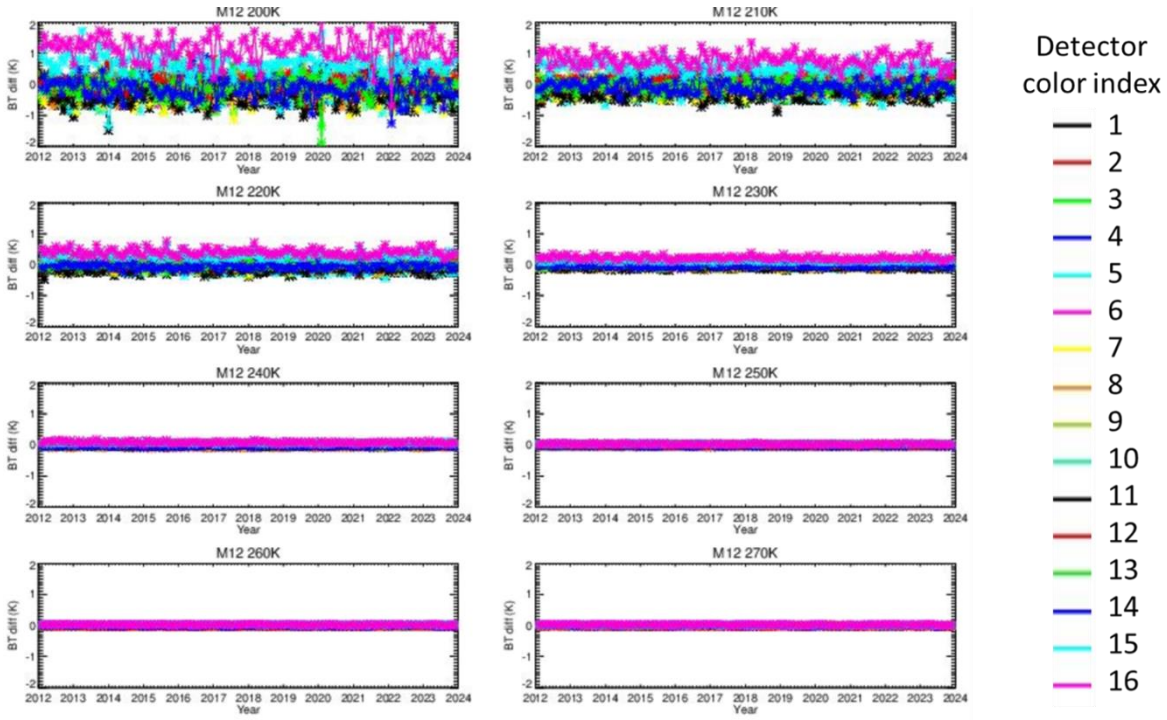

Figure 7. SNPP VIIRS TEB detector difference trending through the end of 2023. Each point is the relative radiance difference for each detector in a two orbit L1B Earth measurement data.

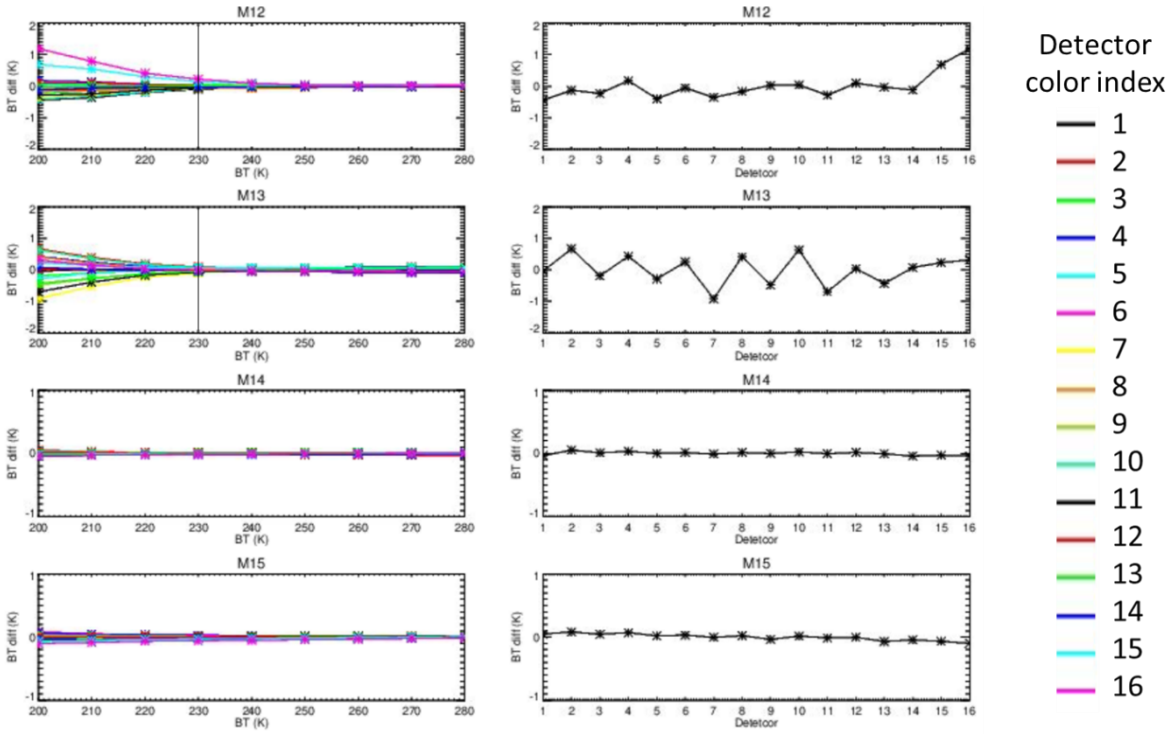

Figure 8. SNPP VIIRS TEB detector difference averaged over entire mission through the end of 2023 as function of BT level. (Left panel) The averaged detector difference as function of scene BT. The vertical lines for M12 and M13 are the minimum temperature measurements in VIIRS specification. For M14 to M16, the minimum temperature in specification is 190K. (Right panel) The average detector difference for each detector.

4.2 N20 VIIRS TEB

Figure 9 shows N20 VIIRS TEB detector difference trending through the end of 2023. Each point is the relative BT difference for each detector in a two orbit L1B Earth measurement data. It also shows that the detector difference is stable over the mission, and the averaged detector difference over the mission can be used for striping assessment. Figure 10 shows N20 VIIRS TEB detector difference averaged over entire mission till end of 2023. The left panel shows the average detector difference as function of scene BT. The right panel shows the average detector difference for each detector. Only the bands M12 and M13 show the relatively larger detector difference for low BT scenes while the other bands detector difference is insignificant. The detector difference is relatively larger for N20 VIIRS TEB, compared with SNPP and N21. Considering the minimum temperature specification is 230 K. the detector difference is still small above 230 K from Figure 10. The edge pixels in zones 1 and 5 have larger noise, and the minimum temperature specification is for these pixels. The pixels in zone 3 are aggregated from 3 original pixels and the noise is lower than the edge pixels. The measurement can be lower than the minimum temperature specification. The offset of the nonlinear response is an important term in the calibration [15]. The assessment lower to 200K can be helpful for calibration improvement. For example, the BT level dependency in Figure 10 shows that the cause of the detector difference may be the offset uncertainty in the nonlinear response function.

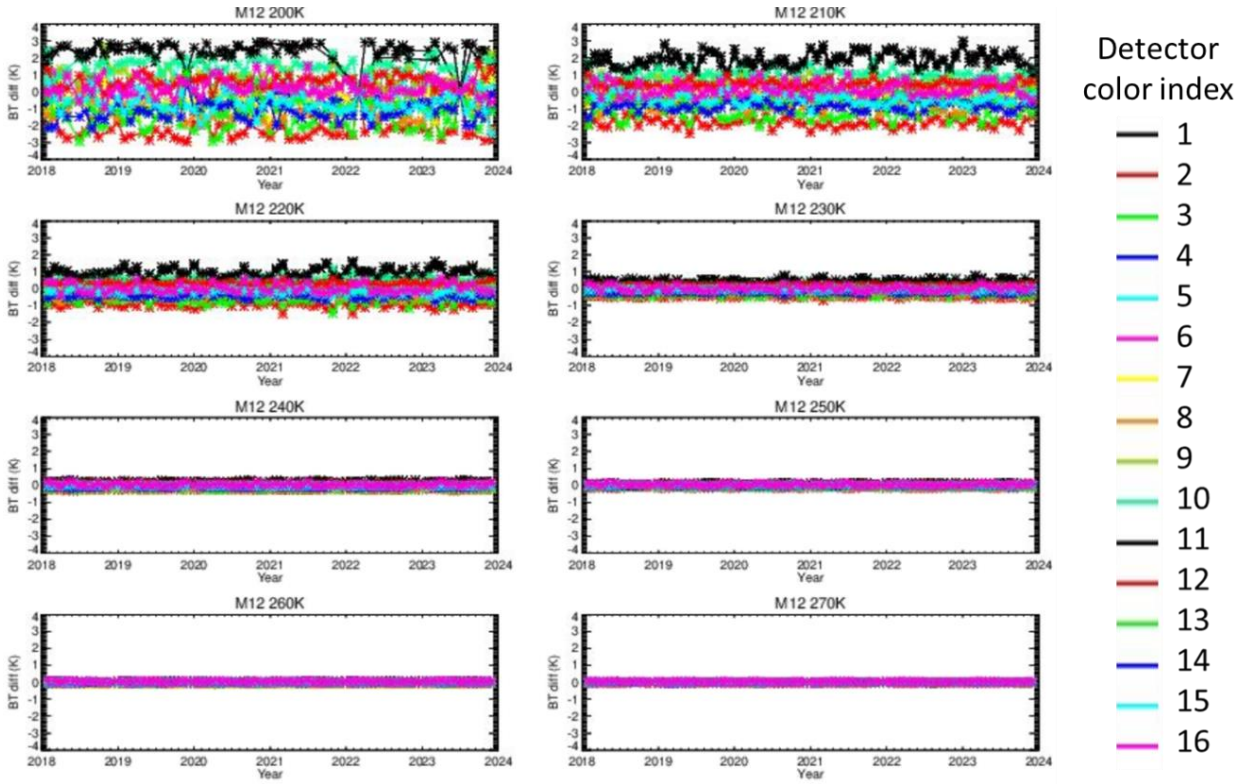

Figure 9. N20 VIIRS TEB detector difference trending until end of 2023. Each point is the relative radiance difference for each detector in a two orbit L1B Earth measurement data.

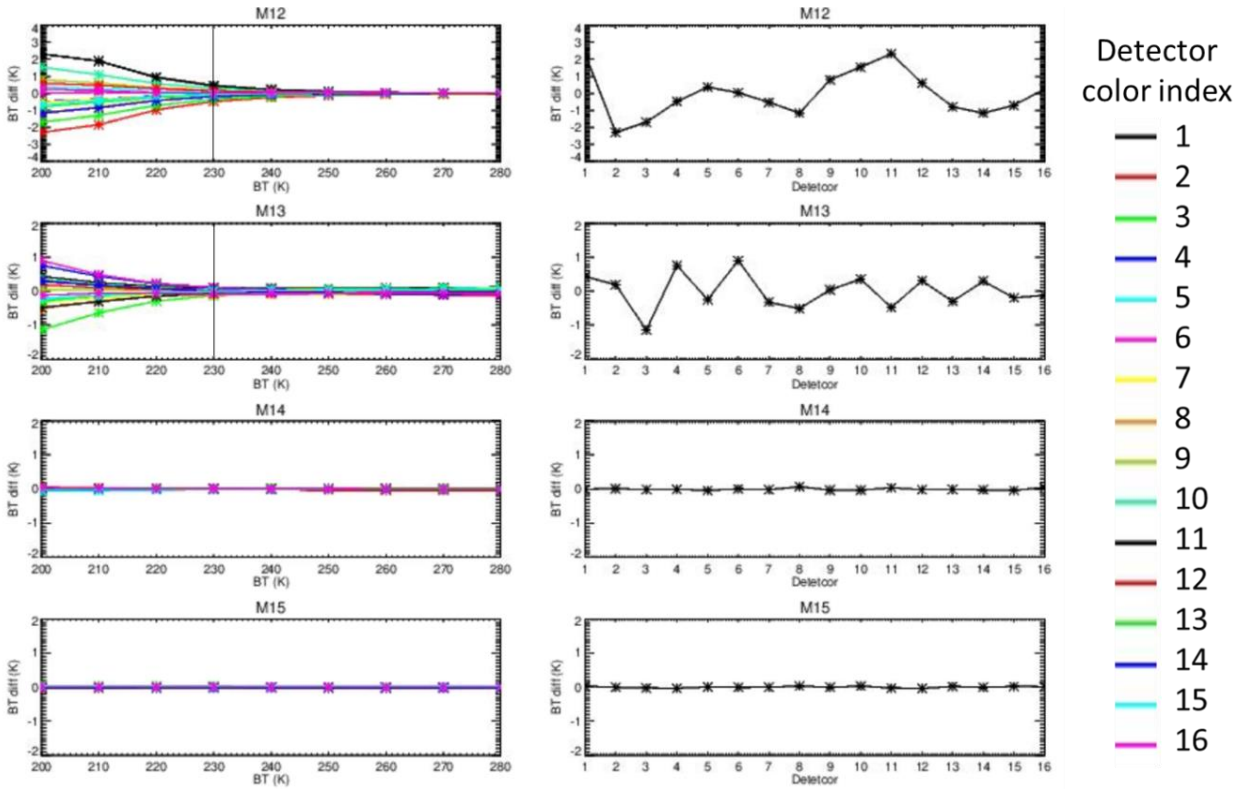

Figure 10. N20 VIIRS TEB detector difference averaged over entire mission until end of 2023 as function of BT level. (Left panel) The averaged detector difference as function of scene BT. The vertical lines for M12 and M13 are the minimum temperature measurements in VIIRS specification. For M14 to M16, the minimum temperature in specification is 190K. (Right panel) The average detector difference for each detector.

4.3 N21 VIIRS TEB

Figure 11 shows N21 VIIRS TEB detector difference trending until end of 2023. Each point is the relative BT difference for each detector in a two orbit L1B Earth measurement data. It also shows that the detector difference is stable over the mission, and the averaged detector difference over the mission can be used for striping assessment. Figure 12 shows N21 VIIRS TEB detector difference averaged over entire mission till end of 2023. The left panel shows the average detector difference as function of scene BT. The right panel shows the average detector difference for each detector. Same as SNPP and N20 VIIRS TEB, only the bands M12 and M13 show the relatively larger detector difference for low BT scenes while the detector difference is insignificant for scene BT above minimum temperature in specification. The other bands detector difference is insignificant. In general, the N21 VIIRS TEB detector difference is insignificant.

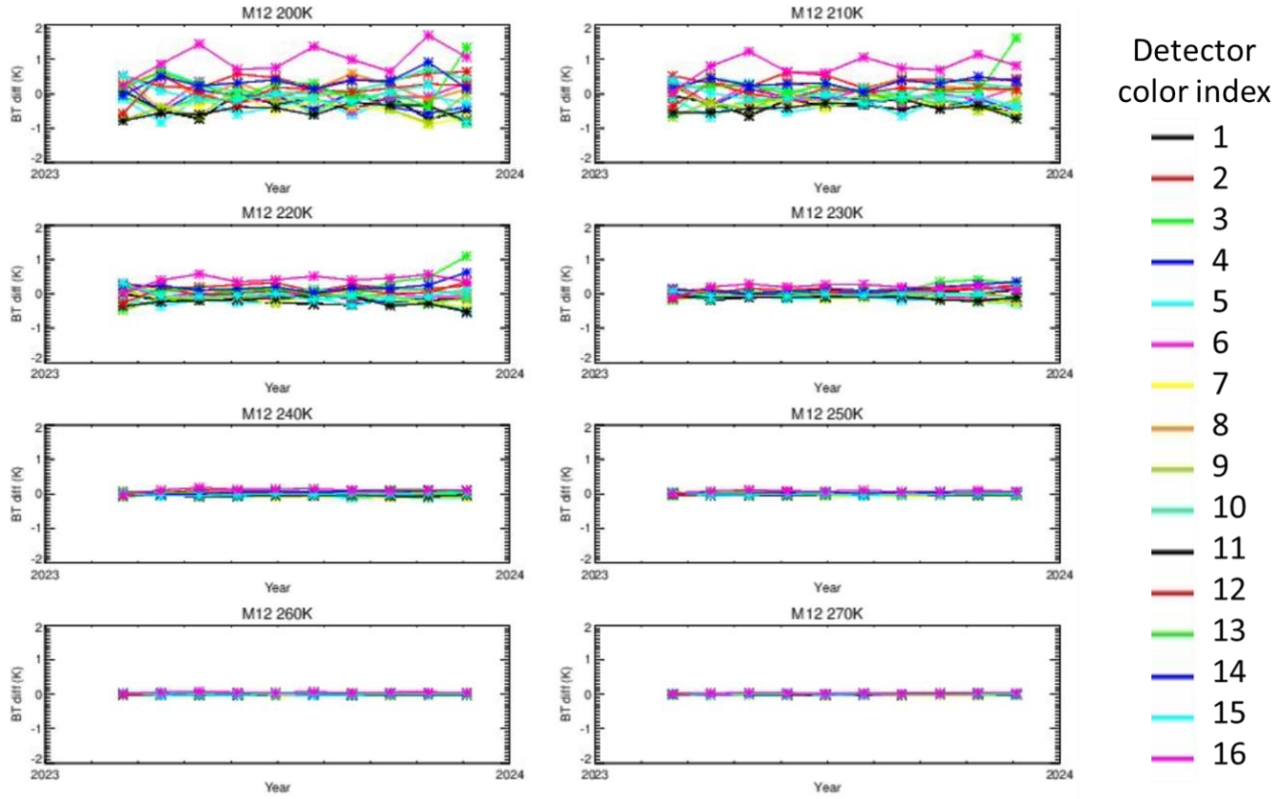

Figure 11. N21 VIIRS TEB detector difference trending until end of 2023. Each point is the relative radiance difference for each detector in a two orbit L1B Earth measurement data.

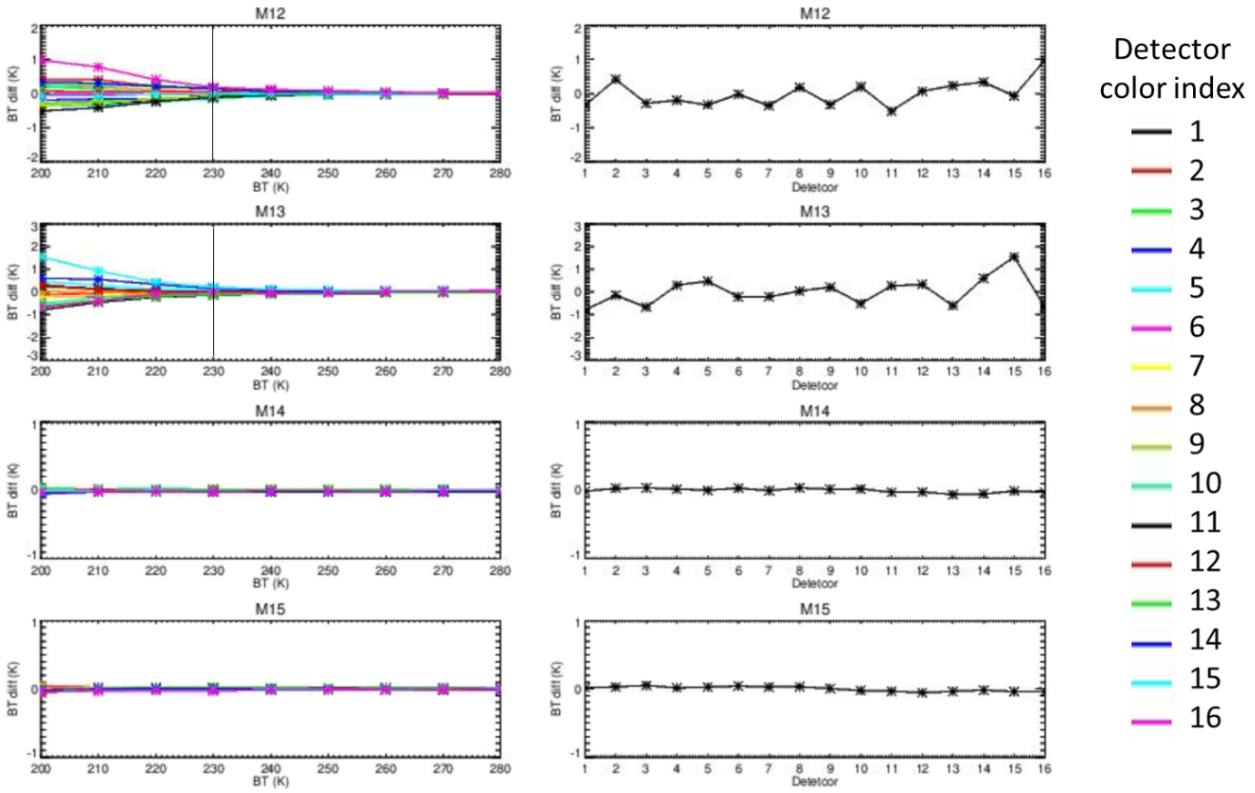

Figure 12. N21 VIIRS TEB detector difference averaged over entire mission until end of 2023 as function of BT level. (Left panel) The averaged detector difference as function of scene BT. The vertical lines for M12 and M13 are the minimum temperature measurements in VIIRS specification. For M14 to M16, the minimum temperature in specification is 190K. (Right panel) The average detector difference for each detector.

5. SUMMARY

The image striping is analyzed for both RSB and TEB of the VIIRS on SNPP, N20, and N21. The method is developed based on the FFT method. The signal level dependency has been processed. The gain stage dependence has been processed. The RSB and TEB M bands have been processed, while the same method can be applied to the I bands in the future. The RSB detector difference of SNPP VIIRS is small for early mission and slightly increases with time. M2 shows a larger increase after 2019, and detector 1 shows the relatively large change. The N20 VIIRS RSB detector difference shows seasonal variation, and the dependency shows that it is mostly for low radiance scenes. It may be related to detector polarization sensitivity or other atmospheric effects. After the de-striping algorithm applied November 2023, the detector difference has been improved for VIS bands. The N21 VIIRS detector difference increases from the start of the mission for most bands. The de-striping algorithm has been applied for the upcoming C2.1 L1B which should significantly reduce the striping in VIS/NIR bands. For VIIRS TEB, detector difference is generally small, and only M12 and M13 shows noticeable detector difference for low BT scenes. Among the three VIIRS instruments, N20 VIIRS M12 and M13 shows the larger detector difference. The minimum temperature specification is 230 K. The detector difference is small above 230 K. The edge pixels in zones 1 and 5 have larger noise, and the minimum temperature specification is for these pixels. The pixels in zone 3 are aggregated from 3 original pixels and the noise is lower than the edge pixels. The measurement can be lower than the minimum temperature specification. The assessment lower to 200 K is helpful to understand the cause of the detector difference and to make calibration improvement if needed.

ACKNOWLEDGMENTS

The authors would like to thank Amit Angal and Kevin Twedt for their internal review of this manuscript. The authors would also like to thank other members of the MODIS Characterization Support Team for their technical assistance and contributions made in support of the MODIS long-term calibration and characterization.

REFERENCES

[1] Xiong X., J. Butler, K. Chiang, B. Efremova, J. Fulbright, N. Lei, J. McIntire, H. Oudrari, J. Sun, Z. Wang, and A. Wu, "VIIRS On-orbit Calibration Methodology and Performance," JGR Vol. 119, Issue 9, pp 5065-5078, 2014

[2] Cao, C., X. Xiong, F. Deluccia, R. Wolfe, and F. Weng, "Early On-Orbit Performance of the Visible Infrared Imaging Radiometer Suite Onboard the Suomi National Polar-Orbiting Partnership (S-NPP) Satellite," IEEE TGRS, vol.52, no.2, pp.1142-1156, 2014

[3] Xiong, X., A. Angal, J. Sun, N. Lei, K. Twedt, and K. Chiang, "Early Results from NOAA-21 (JPSS-2) VIIRS On-orbit Calibration," Proceedings of IGARSS 2023.

[4] Murphy, R.P., P. E. Ardanuy, F. Deluccia, J. E. Clement, and C. Schueler, "The visible infrared imaging radiometer suite, Earth Science Satellite Remote Sensing," vol. 1, New York, USA: Springer-Verlag, pp. 199–223, 2006

[5] Zhou, L., M. Divakarla, X. Liu, et al, "An Overview of the Science Performances and Calibration/Validation of Joint Polar Satellite System Operational Products," Remote Sens., 11, 698, 2019

[6] Goldberg, M. D., H. Kilcoyne, H. Cikanek, and A. Mehta, "Joint Polar Satellite System: The United States next generation civilian polar-orbiting environmental satellite system", J. Geophys. Res.: Atmos., 118(24), 13,463– 13,475, 2013

[7]. Cao, C., F. Deluccia, X. Xiong, R. Wolfe, and F. Weng, "Early On-orbit Performance of the Visible Infrared Imaging Radiometer Suite (VIIRS) onboard the Suomi National Polar-orbiting Partnership (S-NPP) Satellite," IEEE Trans. Geosci. Remote Sens., vol. 52, no.2, pp.1142-1156, doi: 10.1109/TGRS.2013.2247768, 2014

[8] Xiong X., J. Butler, K. Chiang, B. Efremova, J. Fulbright, N. Lei, J. McIntire, H. Oudrari, J. Sun, Z. Wang, and A. Wu, "VIIRS On-orbit Calibration Methodology and Performance," JGR Vol. 119, Issue 9, pp 5065-5078, 2014

[9] Xiong, X., H. Oudrari, J. McIntire, N. Lei, K. Chiang, and A. Angal, "Initial calibration activities and performance assessments of NOAA-20 VIIRS", Proc. SPIE 10781, Earth Observing Missions and Sensors: Development, Implementation, and Characterization V, 107810L, 2018

[10] T. Chang, X. Xiong, and Q. Mu, "VIIRS Reflective Solar Band Radiometric and Stability Evaluation Using Deep Convective Clouds", IEEE Trans. Geosci. Remote Sens., Vol. 54, Issue 12, pp. 7009–7017, 2016

[11] Q. Mu, X. Xiong, A. Wu, and A. Angal, "Assessment of SNPP VIIRS RSB detector-to-detector differences using deep convective clouds and deserts", J. of Appl. Remote Sens., Vol.14, 2020; doi: 10.1117/1.JRS.14.018503.

[12] N. Lei, X. Xiong, Q. Mu, S. Li and T. Chang, "Positional Dependence of SNPP VIIRS Solar Diffuser BRDF Change Factor: An Empirical Approach," in IEEE Transactions on Geoscience and Remote Sensing, vol. 59, no. 10, pp. 8056-8061, 2021, doi: 10.1109/TGRS.2021.3050623

[13] Lin L. and C. Cao, "The Effects of VIIRS Detector-Level and Band-Averaged Relative Spectral Response Differences Between S-NPP and NOAA-20 on the Thermal Emissive Bands", IEEE Journal of selected topics in applied earth observations and remote sensing, Vol. 12, No. 10, 2019

[14] Sun, J., M. Wang, L. Jiang, and X. Xiong, "NOAA-20 VIIRS polarization effect and its correction," Appl. Opt. Vol. 58, No. 24, 6655, 2019

[15] W. Wang, C. Cao and S. Blonski, "Estimating the VIIRS Thermal emissive band response versus scan (RVS) and calibration offsets using on-orbit pitch maneuver data," in IEEE Transactions on Geoscience and Remote Sensing, vol. 60, 1, 2022, doi: 10.1109/TGRS.2022.3181233